PHYSICAL REVIEW D **93,** 055032 (2016)

Interpretation of the diphoton excess at CMS and ATLAS

Bhaskar Dutta,[1] Yu Gao,[1] Tathagata Ghosh,[1] Ilia Gogoladze,[2] and Tianjun Li[3,4]

[1]*Mitchell Institute for Fundamental Physics and Astronomy, Department of Physics and Astronomy, Texas A&M University, College Station, Texas 77843-4242, USA*

[2]*Bartol Research Institute, Department of Physics and Astronomy, University of Delaware, Newark, Delaware 19716, USA*

[3]*State Key Laboratory of Theoretical Physics and Kavli Institute for Theoretical Physics China (KITPC), Institute of Theoretical Physics, Chinese Academy of Sciences, Beijing 100190, People's Republic of China*

[4]*School of Physical Electronics, University of Electronic Science and Technology of China, Chengdu 610054, People's Republic of China*

(Received 17 January 2016; published 22 March 2016)

We consider the diphoton resonance at the 13 TeV LHC in a consistent model with new scalars and vector-like fermions added to the Standard Model, which can be constructed from orbifold grand unified theories and string models. The gauge coupling unification can be achieved, neutrino masses can be generated radiatively, and the electroweak vacuum stability problem can be solved. To explain the diphoton resonance, we study a spin-0 particle, and discuss various associated final states. We also constrain the couplings and number of the introduced heavy multiplets for the new resonance's width at 5 or 40 GeV.

DOI: 10.1103/PhysRevD.93.055032

I. INTRODUCTION

The recent 13 TeV CMS [1] and ATLAS [2] runs have reported a narrow two-photon resonance with an invariant mass near 750 GeV, at a combined 3σ level of credence. Combined with fluctuations from previous 8 TeV data, the excess is reported around 3σ at CMS [3] and 4σ at ATLAS [3].

The narrow diphoton resonance at 750 GeV, if confirmed by future LHC updates, will strongly indicate a massive non-Standard Model (SM) spin-even state. A spin-1 state does not decay into two photons due to the Landau-Yang theorem. An interesting possibility is that the new state X is a SM gauge singlet that couples to the SM particles at the loop level via heavy new-physics scalars and vector-like fermions that are charged under SM gauge groups. As an extension to the SM fermionic sector, we assume a heavy (TeV scale) generation of both quarks and leptons, denoted as Q and L respectively. Their vector-like couplings avoid anomaly. It is also interesting to understand the implications of these states for dark matter, neutrino masses, grand unification, etc. Such kind of models can be realized in the orbifold grand unified theories (GUTs).

In Sec. II we discuss the extensions to the SM and the loop-induced effective couplings. In Sec. III we present the benchmark parameter range of the model to explain the diphoton excess. In Sec. IV we discuss the imminent potential tests of associated collider signals. We further discuss the possibilities of grand unification, neutrino masses, and dark matter, etc., in Sec. V, and then conclude in Sec. VI.

II. AN ECONOMICAL SM EXTENSION

To accommodate for the diphoton signal, we can classify the spins and parities of the resonance particles as 0^+, 0^-, and 2^+, since the vector particle can be excluded due to the Landau-Yang theorem.

First, let us consider the CP-even scalar particle X with mass around 750 GeV, similar to that of the Standard Model Higgs [4–6]. To generate the couplings between X and SM gauge fields, we introduce the vector-like particles F and $\bar{F}$. For simplicity, we only consider the vector-like particles whose quantum numbers are the same as the SM fermions. The relevant Lagrangian is

$$\mathcal{L}_{\rm BSM} = \lambda_F X \bar{F} F + \frac{M_X^2}{2}|X|^2 + M_F \bar{F} F + \text{kinetic terms} \quad (1)$$

where $F = Q$, U, D, L, and E.

For heavy F masses, an effective XVV-type vertex can be induced by F triangle loops in Fig. 1, as

$$\mathcal{L}_{\rm eff} = \kappa_1 X B_{\mu\nu} B^{\mu\nu} + \kappa_2 X W^j_{\mu\nu} W^{j\mu\nu} + \kappa_3 X G^a_{\mu\nu} G^{a\mu\nu}, \quad (2)$$

where $B_{\mu\nu}$, $W^j_{\mu\nu}$ and $G^a_{\mu\nu}$ represent the field-strength tensor of the SM gauge bosons of the $U(1)_Y$, $SU(2)_L$ and $SU(3)_c$ groups, respectively, where $j = 1, 2, 3$ and $a = 1, 2, \ldots 8$ are the indices of the adjoint representations of $SU(2)_L$ and $SU(3)_c$ respectively. We present the κ_i for different F and $\bar{F}$ in Table I.

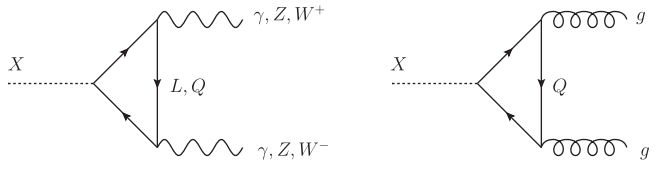

FIG. 1. Heavy fermion loops that couple s to a pair of SM gauge bosons.

TABLE I. The coefficient of κ_is ($i = 1, 2, 3$) for different vector-like particles. Please note the effective couplings κ_i can obtained from the above coefficients by multiplying them by the loop function $A_{1/2}(\tau_F)$ ($F = Q, U, D, L, E$), presented in Eq. (5).

	κ_1	κ_2	κ_3		κ_1	κ_2	κ_3
$(Q, \overline{Q})$	$\frac{\lambda_Q g_Y^2}{96\pi^2 M_Q}$	$\frac{3\lambda_Q g_2^2}{32\pi^2 M_Q}$	$\frac{\lambda_Q g_3^2}{8\pi^2 M_Q}$	$(L, \bar{L})$	$\frac{\lambda_L g_Y^2}{32\pi^2 M_L}$	$\frac{\lambda_L g_2^2}{32\pi^2 M_L}$	0
$(U, \bar{U})$	$\frac{\lambda_U g_Y^2}{12\pi^2 M_U}$	0	$\frac{\lambda_U g_3^2}{16\pi^2 M_U}$	$(E, \bar{E})$	$\frac{\lambda_E g_Y^2}{16\pi^2 M_E}$	0	0
$(D, \bar{D})$	$\frac{\lambda_D g_Y^2}{48\pi^2 M_D}$	0	$\frac{\lambda_D g_3^2}{16\pi^2 M_D}$				

One can also consider the CP-odd scalar particle X with mass around 750 GeV. The relevant Lagrangian is

$$\mathcal{L}_{\rm BSM} = \lambda_F X \bar{F} i\gamma_5 F + \frac{M_X^2}{2}|X|^2 + M_F \bar{F} F + \text{kinetic terms}, \tag{3}$$

where the κ_i for different F and $\bar{F}$ are similar to those in Table I. The CP-odd and -even cases should give identical diphoton signal rates (although the spin correlation in final-state kinematics may differ) and we will restrict to the formalism for the CP-even case after this point. Also, we will use L, Q to denote vector-like new leptons and quarks collectively for collider signal discussions.

The effective couplings of Eq. (2), after rotation to the physical gauge boson states, can be written as,

$$\begin{aligned}
\kappa_{\gamma\gamma} &= \kappa_1 \cos^2\theta_W + \kappa_2 \sin^2\theta_W, \\
\kappa_{ZZ} &= \kappa_2 \cos^2\theta_W + \kappa_1 \sin^2\theta_W, \\
\kappa_{Z\gamma} &= (\kappa_2 - \kappa_1)\sin 2\theta_W, \\
\kappa_{WW} &= 2\kappa_2, \\
\kappa_{gg} &= \kappa_3
\end{aligned} \tag{4}$$

where θ_W is the Weinberg mixing angle. As mentioned before the effective couplings κ_i can be obtained from the coefficients presented in Table I by multiplying them by the loop function, $A_{1/2}(\tau_F)$ (where $F = Q, U, D, L, E$) with a spin-1/2 particle in the loop. The loop function $A_{1/2}(\tau)$ with $\tau = 4M^2/M_X^2$ is given by,

$$A_{1/2}(\tau) = 2\tau[1 + (1-\tau)f(\tau)], \tag{5}$$

with

$$f(x) = \begin{cases} \arcsin^2[1/\sqrt{x}], & \text{if } x \geq 1 \\ -\frac{1}{4}\left[ln\frac{1+\sqrt{1-x}}{1-\sqrt{1-x}} - i\pi\right]^2, & \text{if } x < 1. \end{cases} \tag{6}$$

With the minimal extension of Eq. (1), the lightest neutral component of L, Q (for instance the heavy "neutrino" in an isodoublet L), if present, is stable and can be a dark matter candidate. In the case where the lightest component is charged, it can pair up with a SM fermion into a stable compound state. Alternatively, a small mixing between the heavy L, Q and the SM fermions may be introduced via a Yukawa-type interaction,

$$\begin{aligned}
&y\overline{Q} q_R^{\rm SM} H, \qquad \text{(for isodoublet } Q) \\
&y\overline{Q}^{\rm SM} Q H \qquad \text{(for isosinglet } Q)
\end{aligned} \tag{7}$$

which then allows the heavy Q to decay into their SM fermionic counterparts plus a SM boson. Here we use $Q^{\rm SM}$, $q_R^{\rm SM}$ to denote SM doublet and singlet quarks and H for the Higgs doublet. Q can be strongly pair produced at the LHC and leads to a long-lived ionizing heavy particle (if stable) or a two $2\text{jet} + 2h/2V$ (if unstable) final state. A massive $M_Q > 1$ TeV can be consistent with these bounds (see Ref. [7] and references therein). Similar mixings can also be introduced for L. The heavy leptons are less efficiently produced at the LHC as they do not necessarily have significant mixings with SM leptons, and hence evade excited lepton searches [8]. Analogous slepton search bounds are 260 GeV at CMS [9] and 325 GeV at ATLAS [10], with an assumption of large missing transverse energy in the final state, i.e. a noncompressed scenario. For the study in this paper, vector-like leptons of mass ~400 GeV can be a safe choice above current constraints.

III. THE DIPHOTON SIGNAL

Two of the couplings in Eq. (4), κ_{gg} and $\kappa_{\gamma\gamma}$, can be responsible for the LHC diphoton process as shown in Fig. 2. For a decay width up to a few percent of the mass, the cross section can be given in the narrow-width approximation as

$$\begin{aligned}
\sigma_{\gamma\gamma} &= \frac{\pi^2}{8}\frac{\Gamma(X \to gg)}{M_X} \times \text{BR}(X \to \gamma\gamma) \times \left[\frac{1}{s}\frac{\partial \mathcal{L}_{gg}}{\partial \tau}\right], \\
\frac{\partial \mathcal{L}_{gg}}{\partial \tau} &= \int_0 dx_1 dx_2 f_g(x_1) f_g(X_2) \delta\left(x_1 x_2 - \frac{M_X^2}{s}\right),
\end{aligned} \tag{8}$$

where $\sqrt{s} = 13$ TeV and f_g denotes the gluon parton distribution function inside a proton, with x being the fraction of each beam's energy carried away by the corresponding gluon.

One should note that the experimentally observed width of the resonance is appreciably large. ATLAS suggested a width as large as $\Gamma_X = 6\% M_X$. However, the data collected so far is inconclusive. Reference [11] has performed a

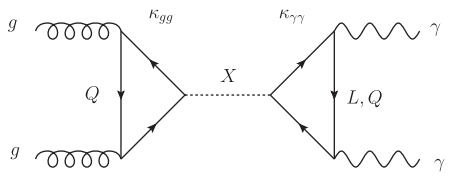

FIG. 2. Loop-level production and diphoton decay of a singlet heavy scalar s.

likelihood analysis to fit both CMS and ATLAS data and checked for their compatibility against the 8 TeV data as well. They have found that for the combined run-I and run-II data, a width of 5 GeV provides almost as good a fit as a width of 40 GeV. Hence, in this analysis we will present benchmark points (BP) with $\Gamma_X = 5$ GeV as well as $\Gamma_X = 40$ GeV. For $\Gamma_X = 5$ GeV Ref. [11] has found the best fit $\sigma_{\gamma\gamma} = 2.4$ fb for $M_X = 750$ GeV. However, a $\sigma_{\gamma\gamma} \sim 0.5$–$4.5$ fb can satisfy the resonance at 95% C.L. In contrast, for $\Gamma_X = 40$ GeV the best fit is obtained for $M_X = 730$ GeV with $\sigma_{\gamma\gamma} = 6$ fb. The corresponding 95% C.L. range is ~2–10 fb. If we fix M_X at 750 GeV the best fit Γ_X and $\sigma_{\gamma\gamma}$ are 30 GeV and 4.8 fb, respectively.

This resonant cross section has the parameter dependence

$$\sigma_{\gamma\gamma} \propto \frac{\kappa_{gg}^2 \kappa_{\gamma\gamma}^2}{\Gamma_X} \propto \frac{\kappa_{gg}^2 \kappa_{\gamma\gamma}^2}{8\kappa_{gg}^2 + \kappa_{\gamma\gamma}^2}, \tag{9}$$

where Γ_X is the total decay width of the resonance. As is evident from Eq. (9), κ_{gg} can be uniquely determined by the experimentally measured $\sigma_{\gamma\gamma}$ in two cases:

(I) only vector-like quarks (Q, U, D) are present in the model and $\kappa_{\gamma\gamma} \propto \kappa_{gg}$;

(II) when $\kappa_{gg} \ll \kappa_{\gamma\gamma}$ where the total width is dominated by large L or E loop contributions.

A. Case I: Vector-like quark-only scenarios

In the Q-only scenario, the correlation between κ_{gg} and $\kappa_{\gamma\gamma}$ is fixed: $\frac{\kappa_{\gamma\gamma}}{\kappa_{gg}} = 0.05$ when Q is an isodoublet, 0.09 when Q is an up-type isosinglet, and 0.02 when it is a down-type isosinglet. For $M_X = 750$ GeV we found that

$$\kappa_{gg} = \begin{cases} 8.7 \times 10^{-5}\ \text{GeV}^{-1}, & \text{doublet} \\ 5.4 \times 10^{-5}\ \text{GeV}^{-1}, & u\text{-type isosinglet} \\ 2.1 \times 10^{-4}\ \text{GeV}^{-1}, & d\text{-type isosinglet} \end{cases} \tag{10}$$

gives the best-fit signal rate of $\sigma_{\gamma\gamma} = 4.8$ fb [11]. The coupling needed for the d-type singlet case is larger due to its small $\kappa_{\gamma\gamma}$ due to reduced electric charge.

In Table II we present two sets of BPs for doublet, u-type isosinglet and d-type isosinglet cases. For the first set, we fix the width to $\Gamma_X = 5$ GeV and evaluate the associated couplings and cross sections in various diboson channels. For the second set of BPs we determine the couplings by fixing $\sigma_{\gamma\gamma} = 4.8$ fb and perform the same calculations. We have set $M_Q = 1$ TeV for both sets of calculations. One can notice from Table II that we need $N_Q \lambda_Q \sim 3 - 17$ to fit either $\Gamma_X = 5$ GeV or $\sigma_{\gamma\gamma} = 4.8$ fb due to small $\kappa_{\gamma\gamma}$ in the Q-only scenarios. Hence, multiple numbers of Q fields are then predicted to keep the coupling λ_Q perturbative. We also show the BR for the decay of X in various diboson channels in Fig. 3. Another alarming prediction from the Q-only scenario is the very small $\text{BR}(X \to \gamma\gamma) < 10^{-3}$ (especially for the down-type Q due to its small electric charge), as shown in Fig. 3. Since $\sigma_{gg} = \sigma_{\gamma\gamma} \frac{\text{BR}(X \to gg)}{\text{BR}(X \to \gamma\gamma)}$, and $\text{BR}(X \to gg) \sim 1$, a very tiny $\text{BR}(X \to \gamma\gamma) < 10^{-2}$ may boost σ_{gg} above the current dijet bound at 2 pb at 8 TeV [12]. We discuss each BP, along with a possible constraint from the aforementioned CMS dijet bound in more detail in the following paragraph.

It is evident from Table II that all BPs that fit $\Gamma_X = 5$ GeV are ruled out by the CMS dijet constraint. In addition for BP-1 and BP-2 the corresponding $\sigma_{\gamma\gamma}$ are too high considering the range described by Ref. [11]. However, BP-3 provides an acceptable value of $\sigma_{\gamma\gamma}$. We do not show any BPs in Table II corresponding to $\Gamma_X = 40$ GeV since the dijet bounds are even worse for them. For $\sigma_{\gamma\gamma} = 4.8$ fb cases, BP-4 and BP-5 are ruled out by the dijet bound but BP-5 survives. However, for BP-5 the total decay width of X is too small (0.79 GeV), but it is within

TABLE II. BPs for Q-only cases with no invisible decay width. Cross sections are calculated in various diboson channels either by keeping $\Gamma_X = 5$ GeV fixed (BP-1,-2,-3) or $\sigma_{\gamma\gamma} = 4.8$ fb fixed (BP-4,-5,-6). We set $M_Q = 1$ TeV for all BPs. Since $\Gamma_X = 5$ GeV BPs are already constrained by dijet bounds, we do not show $\Gamma_X = 40$ GeV BPs in the table since dijet bounds will be even worse for them.

Type	Doublet	u-type singlet	d-type singlet	Doublet	u-type singlet	d-type singlet
Q-only	BP-1	BP-2	BP-3	BP-4	BP-5	BP-6
M_X [GeV]		750			750	
Γ_X [GeV]		5		2.09	0.79	12.7
$N_Q \lambda_Q$	5.18	10.4	10.4	3.35	4.16	16.6
$\kappa_{\gamma\gamma}$ [GeV^{-1}]	7.41×10^{-6}	1.19×10^{-5}	2.99×10^{-6}		4.76×10^{-6}	
κ_{gg} [GeV^{-1}]		1.36×10^{-4}		8.75×10^{-5}	5.44×10^{-5}	2.17×10^{-4}
κ_{WW} [GeV^{-1}]	5.77×10^{-5}	0	0	3.73×10^{-5}	0	0
$\sigma_{\gamma\gamma}$ [fb]	11.9	31.4	1.97		4.8	
σ_{ZZ} [fb]	99.6	2.59	0.16	41.6	0.41	0.41
$\sigma_{Z\gamma}$ [fb]	57.4	18.1	1.13	24	2.87	2.87
σ_{WW} [fb]	337	0	0	141.1	0	0
σ_{gg} [fb]	3.18×10^4	3.27×10^4	3.28×10^4	1.33×10^4	5.21×10^3	8.34×10^4
σ_{gg} (8 TeV) [fb]	6.79×10^3	6.79×10^3	7.00×10^3	2.84×10^3	1.11×10^3	1.79×10^4

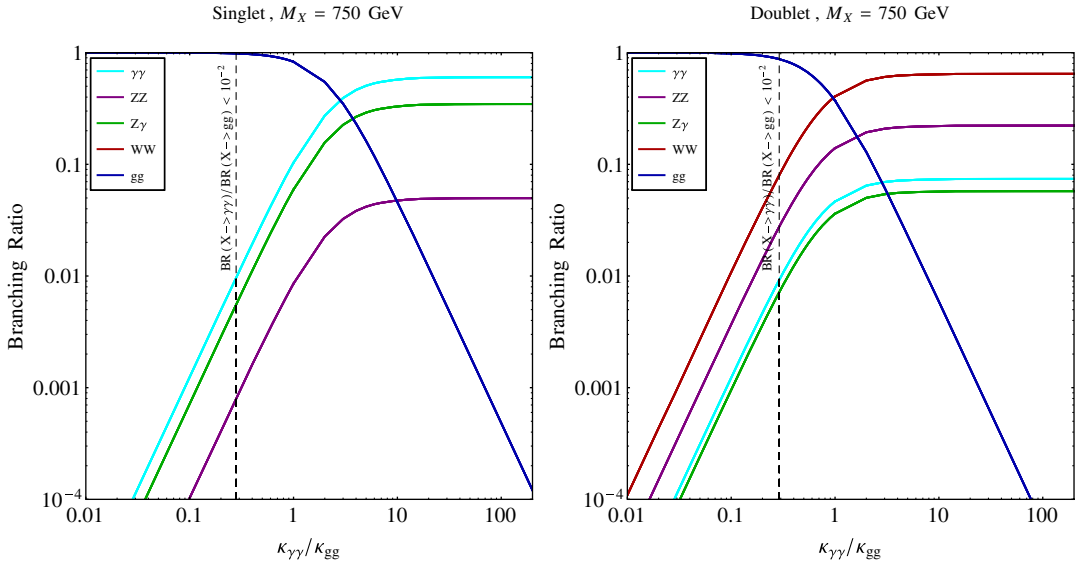

FIG. 3. The 750 GeV scalar decay branchings versus the relative ratio between its coupling to L and Q. The left panel shows the case when L, Q are isosinglets and the right panel shows the isodoublet case.

the 2σ range described by Ref. [11]. One might notice that for the same $\sigma_{\gamma\gamma}$, we need higher κ_{gg} for the doublet compared to the u-type singlet resulting in higher σ_{gg} for the doublet. This is due to the presence of a moderately large Γ_{WW} in the doublet case, which reduces the $\mathrm{BR}(X \to \gamma\gamma)$ and requires a large κ_{gg} to achieve the desired $\sigma_{\gamma\gamma}$ value.

This indicates that extra L species may be required to increase $\mathrm{BR}(X \to \gamma\gamma)$ to simultaneously satisfy $\sigma_{\gamma\gamma} \sim \mathcal{O}(1\text{–}15)$ fb and $\Gamma_X \sim \mathcal{O}(5\text{–}40)$ GeV. Given the early stage of the diphoton resonance measurement, Q-only scenarios can be allowed for a smaller Γ_X, or very large Q hypercharges in other models.

B. Case II: $L \gg Q$ scenarios

When a large L contribution dominates $\kappa_{\gamma\gamma}$ and $\kappa_{\gamma\gamma} \gg \kappa_{gg}$, $\kappa_{\gamma\gamma}$ also disappears from $\sigma_{\gamma\gamma}$, and we found

$$\kappa_{gg} = \begin{cases} 5.8 \times 10^{-6}\ \mathrm{GeV}^{-1}, & \text{doublet} \\ 2.1 \times 10^{-6}\ \mathrm{GeV}^{-1}, & \text{isosinglet} \end{cases} \tag{11}$$

for $\sigma_{\gamma\gamma} = 4.8$ fb. The Γ_X can be greatly enhanced in this scenario by tuning $N_L\lambda_L$ without impacting $\sigma_{\gamma\gamma}$. In Fig. 4 we show the $\sigma_{\gamma\gamma}$ contours for different values of γ_X and the relative strength of couplings of X to photons and gluons. Evidently from Fig. 4, to simultaneously satisfy $\sigma_{\gamma\gamma} \sim \mathcal{O}(1\text{–}15)$ fb and $\Gamma_X \sim \mathcal{O}(5\text{–}40)$ GeV we need a large $\kappa_{\gamma\gamma}$ compared to κ_{gg} for both singlet and doublet cases.

We have noticed in the Q-only case that a loop-induced decay width is often small. With only Q's in the loop, both $\sigma_{\gamma\gamma}$ and Γ_X are determined by κ_{gg} and a very narrow width $\Gamma_X < 1$ GeV is expected to evade the CMS dijet bounds. Additional L species would then be a handy prediction if it is necessary to bring up $\kappa_{\gamma\gamma}$ and Γ_X as illustrated in Fig. 4, and also suppress σ_{gg} at the same time. For a $\Gamma_X \sim 10^{-2} M_X$, we generally need $\kappa_{\gamma\gamma} \sim 10^2 \kappa_{gg}$. Since $\kappa_{\gamma\gamma} \propto N_L\lambda_L$, another prediction is that a significant number of L species must be present ($N_L \gg 1$).

In Table III we again present two sets of BPs for doublet, u-type isosinglet cases.[1] However, as opposed to Table II, in this case our BPs belong to $\Gamma_X = 5$ GeV (BP-7, -8) and $\Gamma_X = 40$ GeV (BP-9, -10) respectively. Due to extra freedom available to us in $L \gg Q$ scenarios, we can easily fit the $\Gamma_X = 40$ GeV width with σ_{gg} being very small. Hence, we do not show any BPs that satisfy $\sigma_{\gamma\gamma} = 4.8$ fb separately since they will be very similar to $\Gamma_X = 40$ GeV cases. Also note that from our discussion earlier in the section that for $\Gamma_X = 40$ GeV the best fit was obtained for $M_X = 730$ GeV by Ref. [11]. So we fix $M_X = 730$ GeV for $\Gamma_X = 40$ GeV BPs, while still using $M_X = 750$ GeV for $\Gamma_X = 5$ GeV BPs for the rest of the paper with best-fit $\sigma_{\gamma\gamma}$ values 2.4 and 6 fb respectively (unless otherwise stated). Along with fixing $M_Q = 1$ TeV, we use $M_L = 400$ GeV for these calculations.

Clearly from Table III we can conclude that we require an unreasonably high value of $N_L\lambda_L$ for all BPs. Hence we need $\mathcal{O}(100)$ copies of vector-like leptons (except for BP-7), assuming perturbativity of λ_L. Nonetheless these BPs do not suffer from dijet bounds. When L, Q loop contributions are comparable in $\kappa_{\gamma\gamma}$, i.e. $N_Q\lambda_Q \sim N_L\lambda_L$, we will again suffer from narrow-width and large dijet cross section problems. We do not discuss this mixed case here for simplicity. However, even in that case we will need many copies of both Q and L, comparable to numbers

[1] d-type isosinglet cases will be similar to u-type cases; only $N_L\lambda_L$ may vary.

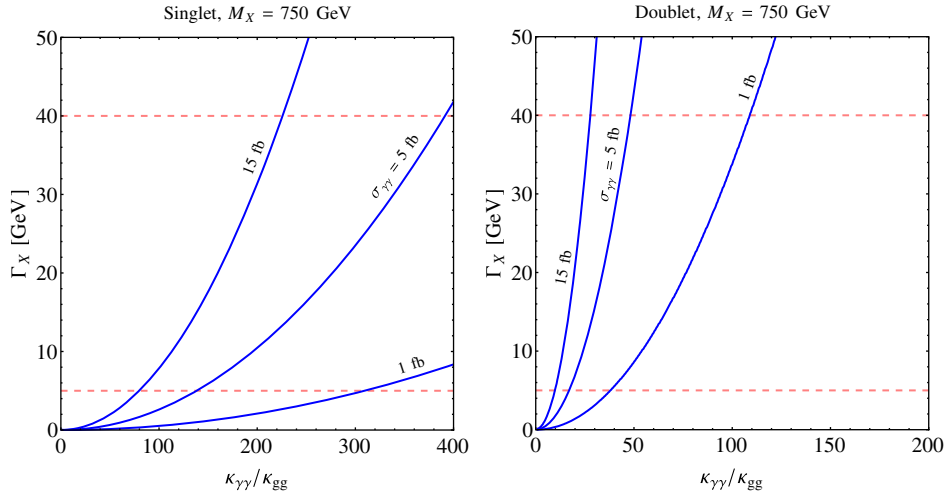

FIG. 4. Diphoton cross section $\sigma_{\gamma\gamma}$ contours for different values of total decay width and the relative strength of couplings of X to photons and gluons. The left panel shows the case when L, Q are isosinglets and the right panel shows the isodoublet case. The pink dashed lines correspond to $\Gamma_X = 5$ GeV (lower) and 40 GeV (upper).

shown in Table II. These many particles potentially require strongly coupled models as discussed in Ref. [13]. Further, with such a large width, the diphoton final state can also be produced via photon fusion which can be established at the ongoing LHC with 20 fb^{-1} of luminosity [14–16].

C. Possible invisible decay of X

To solve the L, Q multiplicity issue, it is possible to couple X to complete SM singlets N, via for instance $X\bar{N}N$, and such an N can have a mass below $M_X/2$ and X can decay into $\bar{N}$, N at tree level. This invisible width can solve the very-narrow-width issue of the new resonance. In this light, an economical setup can be four isodoublet Q and L species to give the correct $\sigma_{\gamma\gamma}$ with a narrow width, and the invisible X decays to accommodate for the measured X width.

If the large decay width mostly arises from the invisible decays of X then we have constraints from the monojet bound as discussed in Ref. [11]. However if this final state also contains a soft lepton ($P_T \sim$ 10–20 GeV), it will not be constrained by the monojet bound [17]. This decay mode can appear if X decays to a pair of fermions (N_2) and each N_2 decays into N_1 and a pair of leptons, where N_1 is the lightest stable particle. This scenario can be realized with an N_2 mass around 300 GeV and an N_1 mass around 250 GeV. The dilepton plus missing energy does not constrain this mode with such a mass gap since the resonance channel produces N_2 back to back and we are left with mostly soft leptons in the final state.

TABLE III. BPs for $L \gg Q$ cases with no invisible decay width. Cross sections are calculated in various diboson channels either for $\Gamma_X = 5$ GeV (BP-7, -8) or $\Gamma_X = 40$ GeV (BP-9, -10). We set $M_Q = 1$ TeV and $M_L = 400$ GeV for all BPs.

Type	Doublet	u-type singlet	Doublet	u-type singlet
$L \gg Q$	BP-7	BP-8	BP-9	BP-10
M_X [GeV]	750		730	
Γ_X [GeV]	5		40	
$N_Q\lambda_Q$	0.17	0.12	0.25	0.18
$N_L\lambda_L$	37	106	113	322
$\kappa_{\gamma\gamma}$ [GeV^{-1}]	1.05×10^{-4}	2.99×10^{-4}	3.10×10^{-4}	8.84×10^{-4}
κ_{gg} [GeV^{-1}]	4.31×10^{-6}	1.50×10^{-6}	6.52×10^{-6}	2.28×10^{-6}
κ_{WW} [GeV^{-1}]	4.57×10^{-4}	0	1.34×10^{-3}	0
$\sigma_{\gamma\gamma}$ [fb]	2.40		6.00	
σ_{ZZ} [fb]	7.28	0.20	18.1	0.49
$\sigma_{Z\gamma}$ [fb]	1.89	1.38	4.70	3.45
σ_{WW} [fb]	21.2	0	52.6	0
σ_{gg} [fb]	0.03	5×10^{-4}	0.02	3×10^{-4}
σ_{gg} (8 TeV) [fb]	7×10^{-4}	1×10^{-4}	5×10^{-3}	7×10^{-5}

TABLE IV. BPs for Q-only cases with large invisible decay width. Cross sections are calculated in various diboson channels by keeping Γ_X fixed at 5 GeV (BP-11, -12, -13) and 40 GeV (BP-14, -15, -16). We set $M_Q = 1$ TeV for all BPs.

Type	Doublet	u-type singlet	d-type singlet	Doublet	u-type singlet	d-type singlet
Q-only with invisible decays	BP-11	BP-12	BP-13	BP-14	BP-15	BP-16
M_X [GeV]		750			730	
Γ_X [GeV]		5			40	
$N_Q\lambda_Q$	3.47	5.49	7.5	6.27	11.6	17.7
$\Gamma_{\rm inv}$ [GeV]	2.76	3.62	2.42	33.3	34.3	26.8
$\kappa_{\gamma\gamma}$ [GeV^{-1}]	4.96×10^{-6}	6.82×10^{-6}	2.15×10^{-6}	8.95×10^{-6}	1.33×10^{-5}	5.06×10^{-6}
κ_{gg} [GeV^{-1}]	9.07×10^{-5}	7.17×10^{-5}	9.80×10^{-5}	1.63×10^{-4}	1.52×10^{-4}	2.31×10^{-4}
κ_{WW} [GeV^{-1}]	3.87×10^{-5}	0	0	6.97×10^{-5}	0	0
$\sigma_{\gamma\gamma}$ [fb]	2.40	2.41	0.52	3.17	6.00	2.02
σ_{ZZ} [fb]	20.0	0.20	0.04	26.4	0.49	0.17
$\sigma_{Z\gamma}$ [fb]	11.6	1.38	0.30	15.2	3.44	1.16
σ_{WW} [fb]	67.9	0	0	89.4	0	0
σ_{gg} [fb]	6.41×10^3	3.51×10^3	8.75×10^3	8.47×10^3	6.25×10^3	3.37×10^4
$\sigma_{\rm inv}$ [fb]	8.01×10^3	6.57×10^3	8.21×10^3	4.26×10^4	3.77×10^4	6.83×10^4
σ_{gg} (8 TeV) [fb]	1.37×10^3	535	1.86×10^3	1.84×10^3	1.36×10^3	7.31×10^3

We present a few more BPs in Tables IV and V, taking into account the large invisible width, for both Q-only and $L \gg Q$ scenarios with $\Gamma_X = 5$ and 40 GeV. Now with the addition of the extra parameter $\Gamma_{\rm inv}$ we can find BPs with $\Gamma_X = 40$ GeV for Q-only cases also. Therefore, similar to Table III, we do not show BPs with $\sigma_{\gamma\gamma} = 4.8$ fb cases.

We see from Table IV that with the introduction of the large invisible width we reduce $N_Q\lambda_Q$ by a factor of ~2 for $\Gamma_X = 5$ GeV. In contrast, for $\Gamma_X = 40$ GeV we still need $N_Q\lambda_Q \sim \mathcal{O}(10)$. Most BPs in Table IV evade the dijet bound of 2 pb at 8 TeV. We note that for BP-13 and BP-15 we tune the parameters to evade the aforementioned bound, which in turn reduces the $\sigma_{\gamma\gamma}$. Nevertheless, the values presented in Table IV are within the 95% C.L. range prescribed by Ref. [11]. However, for BP-16 (d-type quark singlet with $\Gamma_X = 40$ GeV) even for the lowest allowed $\sigma_{\gamma\gamma}$ value, we could not avoid the dijet bound.

In Table V we tabulate BPs with the most economical choice of both $N_Q\lambda_Q$ and $N_L\lambda_L$. The inclusion of the large invisible width reduces the multiplicity of L to a very reasonable level (~2–6). These BPs again evade the dijet bound. Finally, in Figs. 5 and 6, we show the combinations of $N_Q\lambda_Q$ and $N_L\lambda_L$ for the total decay width = 5 and 40 GeV with and without $X \to N\bar{N}$ which we call $\Gamma_{\rm inv}$. We see again that the presence of the invisible width allows us

TABLE V. BPs for $L \gg Q$ cases with large invisible decay width. Cross sections are calculated in various diboson channels either for $\Gamma_X = 5$ GeV (BP-17, -18) $\Gamma_X = 40$ GeV (BP-19, -20). We set $M_Q = 1$ TeV and $M_L = 400$ GeV for all BPs.

Type	Doublet	u-type singlet	Doublet	u-type singlet
$L \gg Q$ with invisible decays	BP-17	BP-18	BP-19	BP-20
M_X [GeV]	750		730	
Γ_X [GeV]	5		40	
$N_Q\lambda_Q$	2.02	2.92	4.30	6.30
$N_L\lambda_L$	2.00	3.00	4.31	6.30
$\Gamma_{\rm inv}$ [GeV]	4.2	4.6	36.7	38.3
$\kappa_{\gamma\gamma}$ [GeV^{-1}]	8.53×10^{-6}	1.18×10^{-5}	1.80×10^{-5}	2.45×10^{-5}
κ_{gg} [GeV^{-1}]	5.28×10^{-5}	3.82×10^{-5}	1.12×10^{-4}	8.22×10^{-5}
κ_{WW} [GeV^{-1}]	4.69×10^{-5}	0	9.90×10^{-5}	0
$\sigma_{\gamma\gamma}$ [fb]	2.40		6.00	
σ_{ZZ} [fb]	10.8	0.20	27.1	0.49
$\sigma_{Z\gamma}$ [fb]	4.22	1.38	10.6	3.44
σ_{WW} [fb]	33.9	0	84.7	0
σ_{gg} [fb]	736	201	1.87×10^3	540
$\sigma_{\rm inv}$ [fb]	4.13×10^3	2.37×10^3	2.21×10^4	1.24×10^4
σ_{gg} (8 TeV) [fb]	157	43	407	117

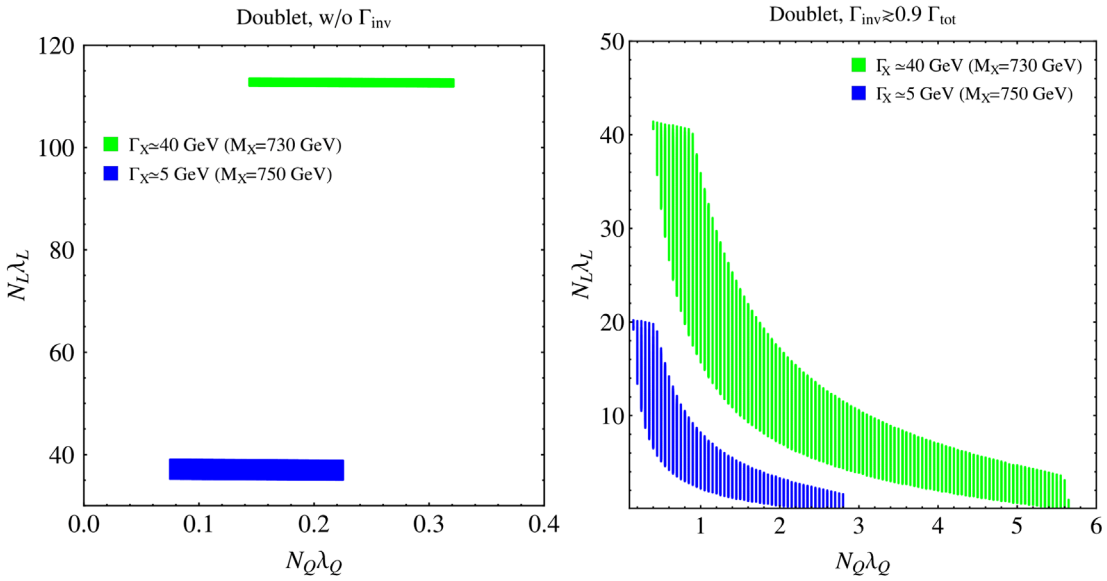

FIG. 5. Doublet $N_L\lambda_L$, $N_Q\lambda_Q$ ranges for different values of the resonance width. The left panel assumes no invisible decays and the right panel assumes a dominant invisible width of X.

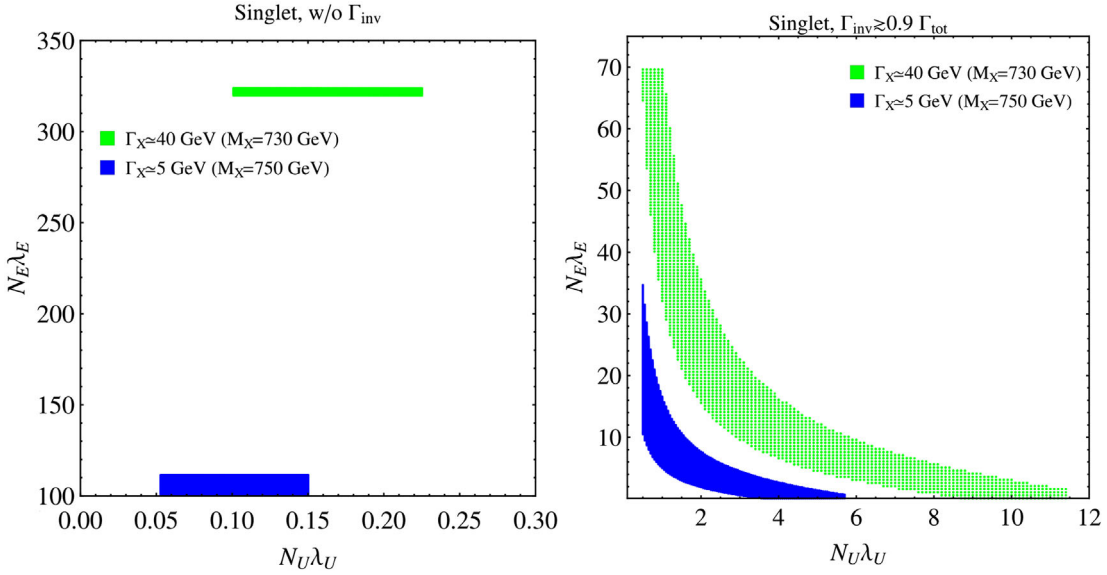

FIG. 6. Singlet $N_L\lambda_L$, $N_Q\lambda_Q$ ranges for different values of the resonance width. The left panel assumes no invisible decays and the right panel assumes a dominant invisible width of X.

to fit the width with smaller values of $N_Q\lambda_Q$ and $N_L\lambda_L$ both for doublet and singlet fields.

IV. ASSOCIATED COLLIDER TESTS

If the 750 GeV diphoton excess persists, a few associated signals would be expected from the mixing between the SM gauge fields:

(i) $X \to ZZ, Z\gamma$ decays, leading to $4l$, $2l + \not{E}_T/\gamma, \gamma + \not{E}_T$ channels.

(ii) An $X \to W^+W^-$ final state if L and/or Q is an isospin doublet.

The expected signal cross section is readily given by $\sigma_{VV} = \sigma_{\gamma\gamma}\frac{\mathrm{BR}(X\to VV)}{\mathrm{BR}(X\to\gamma\gamma)}$, multiplied by further decay branchings of the SM vector bosons. Here we list the leading predicted signals in Table VI for all BPs considered in the previous section that survive the CMS dijet bound. The presence of such associated decays should serve as a good test of the SM gauge mixing, if the 750 GeV resonance is established in the future data. Alternatively, these ZZ, $Z\gamma$ channels can help confirm/rule out new-physics scenarios, e.g. our weakly charged vector-like heavy fermion hypothesis.

TABLE VI. A few leading test channels arising from associated $X \to VV$ decays, for BPs which survive the CMS dijet bound. Here $l = e, \mu$ refers only to the first two generations of leptons, and E_T arises from neutrinos. All the cross sections are in fb.

Channel	$ZZ \to 4l$	$ZZ \to 2l + E_T$	$Z\gamma \to \gamma + 2l$	$Z\gamma \to \gamma + \not{E}_T$	$WW \to e\mu + \not{E}_T$
BR	0.45%	2.7%	6.7%	20%	2.3%
Note	Two pairs of $M_{ll} = M_Z$	$M_{ll} = M_Z$	Monophoton,$M_{ll} = M_Z$	Monophoton with large $\not{E}_T$	Different l flavor
BP-5	0.002	0.01	0.19	0.57	0
BP-7	0.03	0.20	0.13	0.38	0.49
BP-8	0.0009	0.005	0.09	0.28	0
BP-9	0.08	0.49	0.31	0.94	1.21
BP-10	0.002	0.01	0.23	0.69	0
BP-11	0.09	0.54	0.78	2.32	1.56
BP-12	0.0009	0.005	0.09	0.28	0
BP-13	0.0002	0.001	0.02	0.06	0
BP-14	0.12	0.71	1.02	3.04	2.06
BP-15	0.002	0.01	0.23	0.69	0
BP-17	0.05	0.29	0.28	0.84	0.78
BP-18	0.0009	0.005	0.09	0.28	0
BP-19	0.12	0.73	0.71	2.12	1.95
BP-20	0.002	0.01	0.23	0.69	0

The $4l$ and the monophoton $+ \not{E}_T$ channels are probably the most imminent tests of the associated $X \to ZZ$, $Z\gamma$ decays. In current data, CMS [18] constrains a ZZ resonance at 750 GeV to be less than 0.12 pb. The associated monophoton signal in the Q-only doublet cases are close to being constrained but are within the existing CMS [19] limits. Future updates from 13 TeV runs would strongly constrain or confirm these associated signals.

V. THEORETICAL DISCUSSIONS

There are many motivations to look beyond the SM physics, namely neutrino masses and mixings, dark matter, gauge coupling unification and the SM Higgs mass vacuum stability. Recently, the CMS and ATLAS collaborations announced an excess in the distribution of events containing two photons peaked at 750 GeV or so which can be interpreted as new motivation for physics beyond the SM. Our goal in this paper is to connect all of the above-mentioned motivations for new physics to each other.

It was shown some time ago that demanding gauge coupling unification to be consistent with the proton decay constraint can lead to the simplest and most minimal extension of the SM as follows:

$$Q_f\left(3,2,\frac{1}{6}\right) + \overline{Q}_f\left(\bar{3},2,-\frac{1}{6}\right) + D_s^c\left(3,1,-\frac{1}{3}\right) + U_s^c\left(3,1,\frac{2}{3}\right) + L_s^c\left(1,2,\frac{1}{2}\right), \tag{12}$$

where subscripts s and f are for scalars and fermions of new particles. We would like to emphasize that this model can be realized in the orbifold GUTs. The result obtained from performing the two-loop renormalization group equation (RGE) evaluation is presented in Fig. 7.

As shown in Ref. [20] the neutrino masses and mixings can be generated radiatively using the Lagrangian

$$\mathcal{L} \supset M_Q Q\overline{Q} + M_{D^c}^2|D_s^c|^2 + M_{U^c}^2|U_s^c|^2 + \lambda_1 QLD_s^c + \Lambda_2 \overline{Q}LU_s^{c*} + \lambda D_s^c U_s^{c*} H^2. \tag{13}$$

The loop involves the colored particle presented in Eq. (12) (shown in Fig. 8) and the expression for the neutrino mass:

$$\mathcal{M}_\nu \simeq \frac{\lambda_1\lambda_2}{16\pi^2}\frac{\lambda\langle H\rangle^2}{M_{D^c}^2 - M_{U^c}^2} \times \left(\frac{M_{D^c}^2 M_Q}{M_Q^2 - M_{D^c}^2}\log\frac{M_Q^2}{M_{D^c}^2} - \frac{M_{U^c}^2 M_Q}{M_Q^2 - M_{U^c}^2}\log\frac{M_Q^2}{M_{U^c}^2}\right) \tag{14}$$

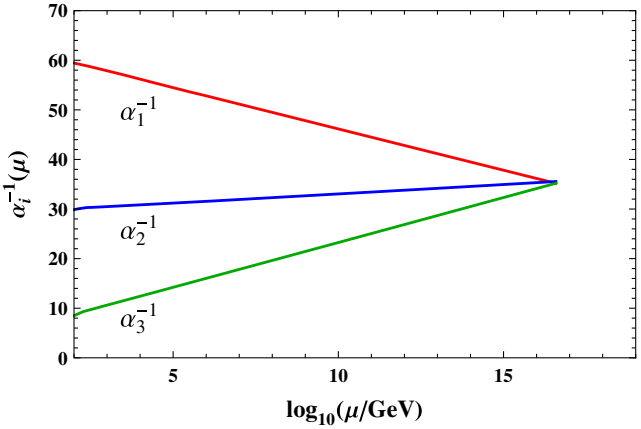

FIG. 7. Gauge coupling unification at two loops involving fermions $[Q(3,2,1/6) + \overline{Q}(\bar{3},2,-1/6)]$, and scalars $[D_s^c(3,1,-1/3) + U_s^c(3,1,2/3)]$. Unification happens at 7×10^{15} GeV with $\alpha^{-1} = 36$.

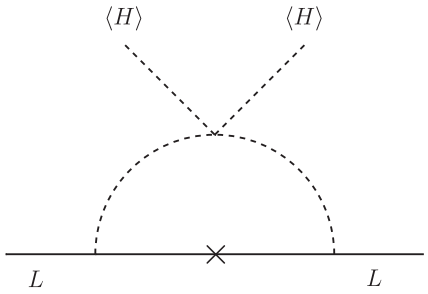

FIG. 8. One loop diagram for generating neutrino masses.

On the other hand, having a stable scalar doublet in the spectrum can be interpreted as an inert doublet model for dark matter [21]. The charge neutral component of the doublet can be lighter than the charged component due to radiative corrections [22]. Also it is very interesting to note that having this [see Eq. (12)] new particle in the spectrum can solve the Higgs vacuum stability problem [23]. It is very interesting to note that all of this new-physics motivation can lead to the prediction of the diphoton excess which we hope will be confirmed in the near future.

We would like to point out that the generic vector-like particles do not need to form complete $SU(5)$ or $SO(10)$ representations in GUTs from the orbifold constructions [24–26], the intersecting D-brane model building on Type II orientifolds [27–29], M-theory on S^1/Z_2 with Calabi-Yau compactifications [30,31], and F-theory with $U(1)$ fluxes [32–35] (see Ref. [36] and references therein.)

The generic vector-like particles from orbifold GUTs and F-theory GUTs have been studied previously in Refs. [36–38]. From Ref. [36], we found that in the orbifold GUTs, we cannot realize such a set of vector-like particles and scalars since the scalar U_s^c cannot be obtained. Interestingly, in the F-theory $SU(5)$ models, we can indeed realize such a set of vector-like particles and scalars. For details, please see Table IV in Ref. [36]. Moreover, without additional vector-like particles or scalars, the GUT scale is still around 7×10^{15} GeV, and the GUT gauge coupling α is about $1/36$. Thus, the proton lifetime via dimension-six operators will be within the reach of the future Super-Kamiokande and Hyper-Kamiokande experiments.

VI. CONCLUSION

We proposed a new model from orbifold GUTs/string models to explain the recent diphoton resonance at the LHC by introducing new scalars and vector-like fermions. We showed that it is possible to explain the diphoton resonance, and such an explanation for the diphoton resonance does not conflict with any other bound. Interestingly, the upcoming results can constrain some of these explanations. We investigated the number of copies of new particles needed to explain the excess. We noticed that the new fermions and scalars also provide us with the grand unification of gauge couplings. Further, the new fields also generate neutrino masses and the noncolored doublet provides the dark matter candidate. In addition the vector-like fields also provide the stability of the electroweak vacuum since the SM gauge couplings become strong at a high scale via RGE running. We showed the constraints on the new couplings and a number of new multiplets.

ACKNOWLEDGMENTS

We thank Ali Celic, Mykhailo Dalchenko and Teruki Kamon for helpful discussions. This work is supported by DOE Grant No. DE-FG02-13ER42020 (B. D., T. G.), Natural Science Foundation of China under Grants No. 11135003, No. 11275246, and No. 11475238 (T. L.) and support from the Mitchell Institute. Y. G. thanks the Mitchell Institute for Fundamental Physics and Astronomy for support. I. G. thanks the Bartol Research Institute for partial support.

Note added.—While we were completing the draft, we noticed a few papers [13,39–50] appeared in the arXiv on the same topic.

[1] CMS note, CMS PAS EXO-15-004.
[2] ATLAS note, ATLAS-CONF-2015-081.
[3] J. Olsen and M. Kado, ATLAS and CMS physics results from Run 2, available at https://indico.cern.ch/event/442432/.
[4] D. Carmi, A. Falkowski, E. Kuflik, T. Volansky, and J. Zupan, J. High Energy Phys. 10 (2012) 196.
[5] N. Bonne and G. Moreau, Phys. Lett. B **717**, 409 (2012).
[6] J. A. Aguilar-Saavedra, R. Benbrik, S. Heinemeyer, and M. Pérez-Victoria, Phys. Rev. D **88**, 094010 (2013).
[7] https://atlas.web.cern.ch/Atlas/GROUPS/PHYSICS/CombinedSummaryPlots/EXOTICS/index.html#ATLAS_Exotics_Summary.
[8] V. Khachatryan *et al.* (CMS Collaboration), arXiv:1511.01407.
[9] V. Khachatryan *et al.* (CMS Collaboration), Eur. Phys. J. C **74**, 3036 (2014).
[10] G. Aad *et al.* (ATLAS Collaboration), J. High Energy Phys. 05 (2014) 071.
[11] A. Falkowski, O. Slone, and T. Volansky, J. High Energy Phys. 02 (2016) 152.

[12] CMS Collaboration [CMS Collaboration], CMS-PAS-EXO-14-005.
[13] R. Franceschini *et al.*, arXiv:1512.04933.
[14] S. Fichet, G. von Gersdorff, and C. Royon, arXiv:1512.05751.
[15] C. Csáki, J. Hubisz, and J. Terning, Phys. Rev. D **93**, 035002 (2016).
[16] C. Csaki, J. Hubisz, S. Lombardo, and J. Terning, arXiv:1601.00638.
[17] B. Dutta, Y. Gao, T. Ghosh, I. Gogoladze, T. Li, Q. Shafi, and J. W. Walker, arXiv:1601.00866.
[18] S. Chatrchyan *et al.* (CMS Collaboration), J. High Energy Phys. 02 (2013) 036.
[19] V. Khachatryan *et al.* (CMS Collaboration), Phys. Lett. B **755**, 102 (2016).
[20] K. S. Babu and J. Julio, Phys. Rev. D **85**, 073005 (2012).
[21] E. Ma, Phys. Rev. D **73**, 077301 (2006).
[22] C. Garcia-Cely, M. Gustafsson, and A. Ibarra, J. Cosmol. Astropart. Phys. 02 (2016) 043; F. S. Queiroz and C. E. Yaguna, J. Cosmol. Astropart. Phys. 02 (2016) 038.
[23] I. Gogoladze, B. He, and Q. Shafi, Phys. Lett. B **690**, 495 (2010).
[24] Y. Kawamura, Prog. Theor. Phys. **103**, 613 (2000); **105**, 999 (2001); **105**, 691 (2001).
[25] G. Altarelli and F. Feruglio, Phys. Lett. B **511**, 257 (2001).
[26] L. Hall and Y. Nomura, Phys. Rev. D **64**, 055003 (2001).
[27] R. Blumenhagen, M. Cvetic, P. Langacker, and G. Shiu, Annu. Rev. Nucl. Part. Sci. **55**, 71 (2005) and references therein.
[28] M. Cvetic, I. Papadimitriou, and G. Shiu, Nucl. Phys. **B659**, 193 (2003); **B696**, 298(E) (2004).
[29] C. M. Chen, T. Li, and D. V. Nanopoulos, Nucl. Phys. **B751**, 260 (2006).
[30] V. Braun, Y. H. He, B. A. Ovrut, and T. Pantev, Phys. Lett. B **618**, 252 (2005); J. High Energy Phys. 05 (2006) 043 and references therein.
[31] V. Bouchard and R. Donagi, Phys. Lett. B **633**, 783 (2006) and references therein.
[32] R. Donagi and M. Wijnholt, Adv. Theor. Math. Phys. **15**, 1237 (2011).
[33] C. Beasley, J. J. Heckman, and C. Vafa, J. High Energy Phys. 01 (2009) 058.
[34] C. Beasley, J. J. Heckman, and C. Vafa, J. High Energy Phys. 01 (2009) 059.
[35] R. Donagi and M. Wijnholt, Adv. Theor. Math. Phys. **15**, 1523 (2011).
[36] T. Li and D. V. Nanopoulos, J. High Energy Phys. 10 (2011) 090.
[37] J. Jiang, T. Li, D. V. Nanopoulos, and D. Xie, Nucl. Phys. **B830**, 195 (2010).
[38] T. Li, Phys. Rev. D **81**, 065018 (2010).
[39] K. Harigaya and Y. Nomura, Phys. Lett. B **754**, 151 (2016).
[40] Y. Mambrini, G. Arcadi, and A. Djouadi, arXiv:1512.04913.
[41] M. Backovic, A. Mariotti, and D. Redigolo, arXiv:1512.04917.
[42] A. Angelescu, A. Djouadi, and G. Moreau, arXiv:1512.04921.
[43] Y. Nakai, R. Sato, and K. Tobioka, arXiv:1512.04924.
[44] S. Knapen, T. Melia, M. Papucci, and K. Zurek, arXiv:1512.04928.
[45] D. Buttazzo, A. Greljo, and D. Marzocca, Eur. Phys. J. C **76**, 116 (2016).
[46] A. Pilaftsis, Phys. Rev. D **93**, 015017 (2016).
[47] S. Di Chiara, L. Marzola, and M. Raidal, arXiv:1512.04939.
[48] S. D. McDermott, P. Meade, and H. Ramani, Phys. Lett. B **755**, 353 (2016).
[49] A. Kobakhidze, F. Wang, L. Wu, J. M. Yang, and M. Zhang, arXiv:1512.05585.
[50] A. Ahmed, B. M. Dillon, B. Grzadkowski, J. F. Gunion, and Y. Jiang, arXiv:1512.05771.